Ultrahigh Mass Loading, Binder-Free Synthetic Approach for Mesoporous Graphitic Carbon in 3D Current Collector for High Energy Lithium-Ion Batteries

Jun Kim[†, ψ, 1], *Keon-Woo Kim*[†, ψ, 1], *Hyeongkeon Yoon*[†, ψ], *Shin Park*[€], *Dokyung Woo*[†, ψ], *Hangjun Jo*[†, ψ], *Changshin Jo*[*, €, ψ], *Jin Kon Kim*[*, †, ψ]

[†]National Creative Research Initiative Center for Hybrid Nano Materials by High-level Architectural Design of Block Copolymer

[ψ]Department of Chemical Engineering, Pohang University of Science and Technology (POSTECH), Pohang, Gyeongbuk 790-784, Republic of Korea

[€]Department of Battery Engineering, Pohang University of Science and Technology (POSTECH), Pohang, Gyeongbuk 790-784, Republic of Korea

[1]Theses authors contributed equally to this work

Corresponding Authors: jochangshin@postech.ac.kr **(C.J),** jkkim@postech.ac.kr **(J.K.K)**

Keywords: Lithium ion batteries, Conductive carbon, Binder-free, High-mass loading, Mesoporous materials

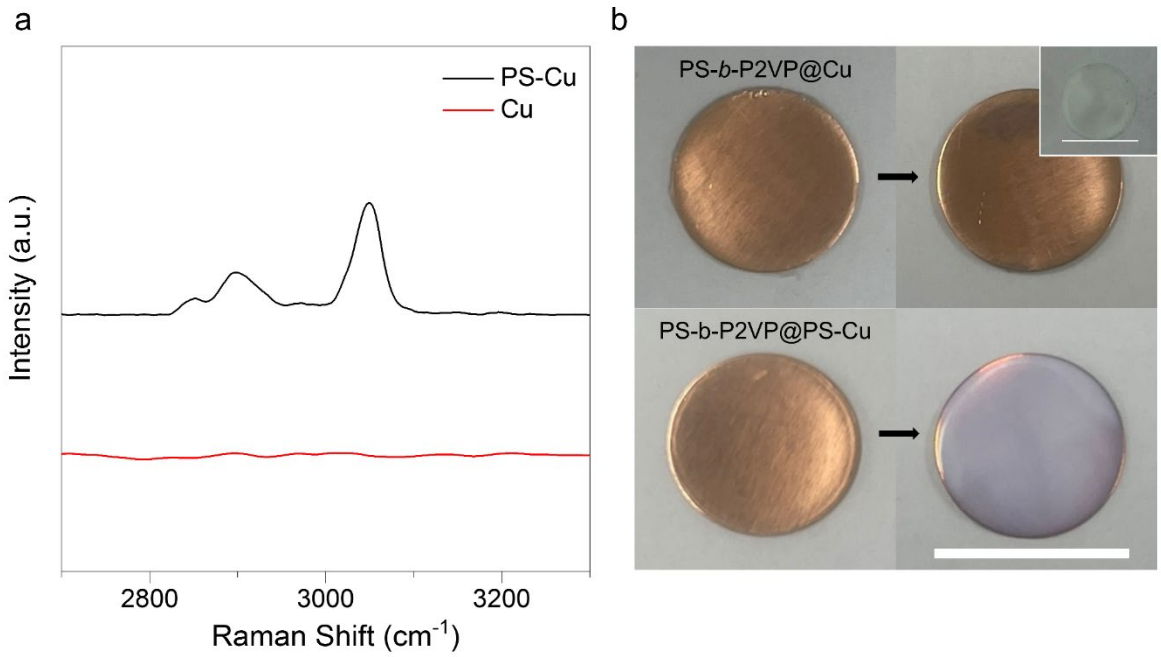

Figure S1 (a) Raman spectra of 3D Cu before and after grafting PS-OH on 3D Cu. The characteristic peaks of PS at 2850 cm^{-1}, 2900 cm^{-1}, and 3050 cm^{-1} are clearly seen.[1] (b) Photographs showing the effect of the PS brush on the adhesion of PS-*b*-P2VP on 3D Cu. In the absence of the PS brush, the PS-*b*-P2VP film delaminated from pristine Cu during ethanol swelling (top images). However, no delamination of the PS-*b*-P2VP film occurred on PS-Cu (bottom images), indicating that PS grafting is essential for a good adhesion of PS-*b*-P2VP with 3D Cu. (all scale bars: 1.5 cm)

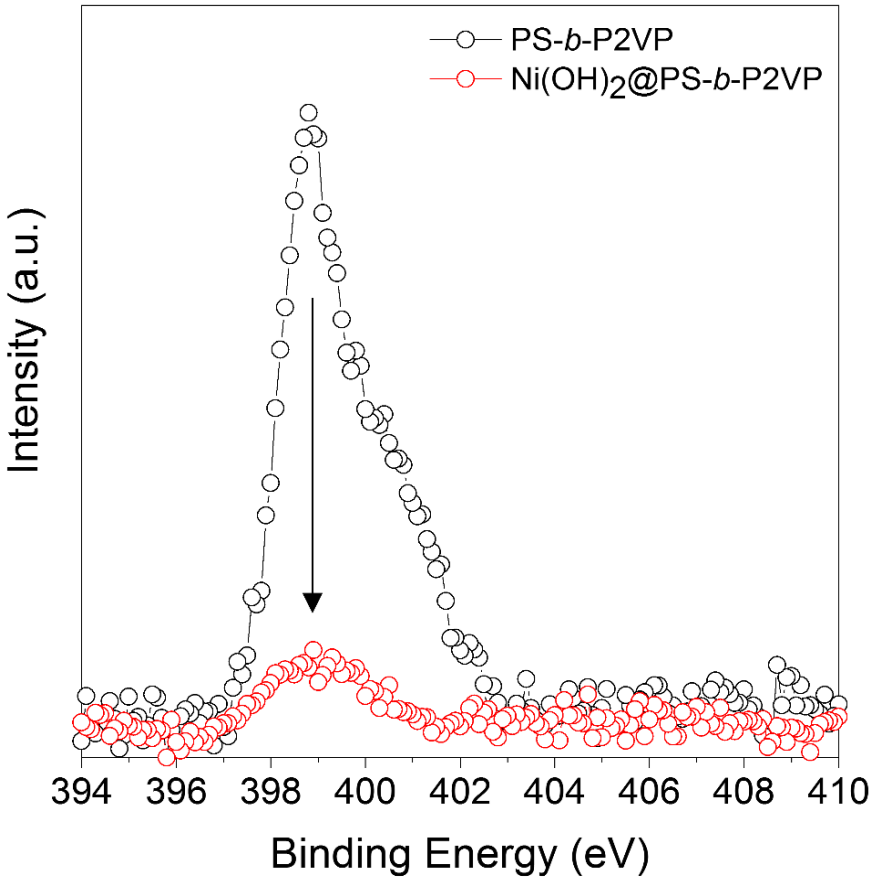

Figure S2 Comparison of X-ray photoelectron spectroscopy (XPS) N 1s spectra for PS-*b*-P2VP and $Ni(OH)_2$@PS-*b*-P2VP. A significantly reduced N peak corresponding to the pyridinic nitrogen of P2VP is observed for $Ni(OH)_2$@PS-*b*-P2VP due to the coverage by $Ni(OH)_2$.

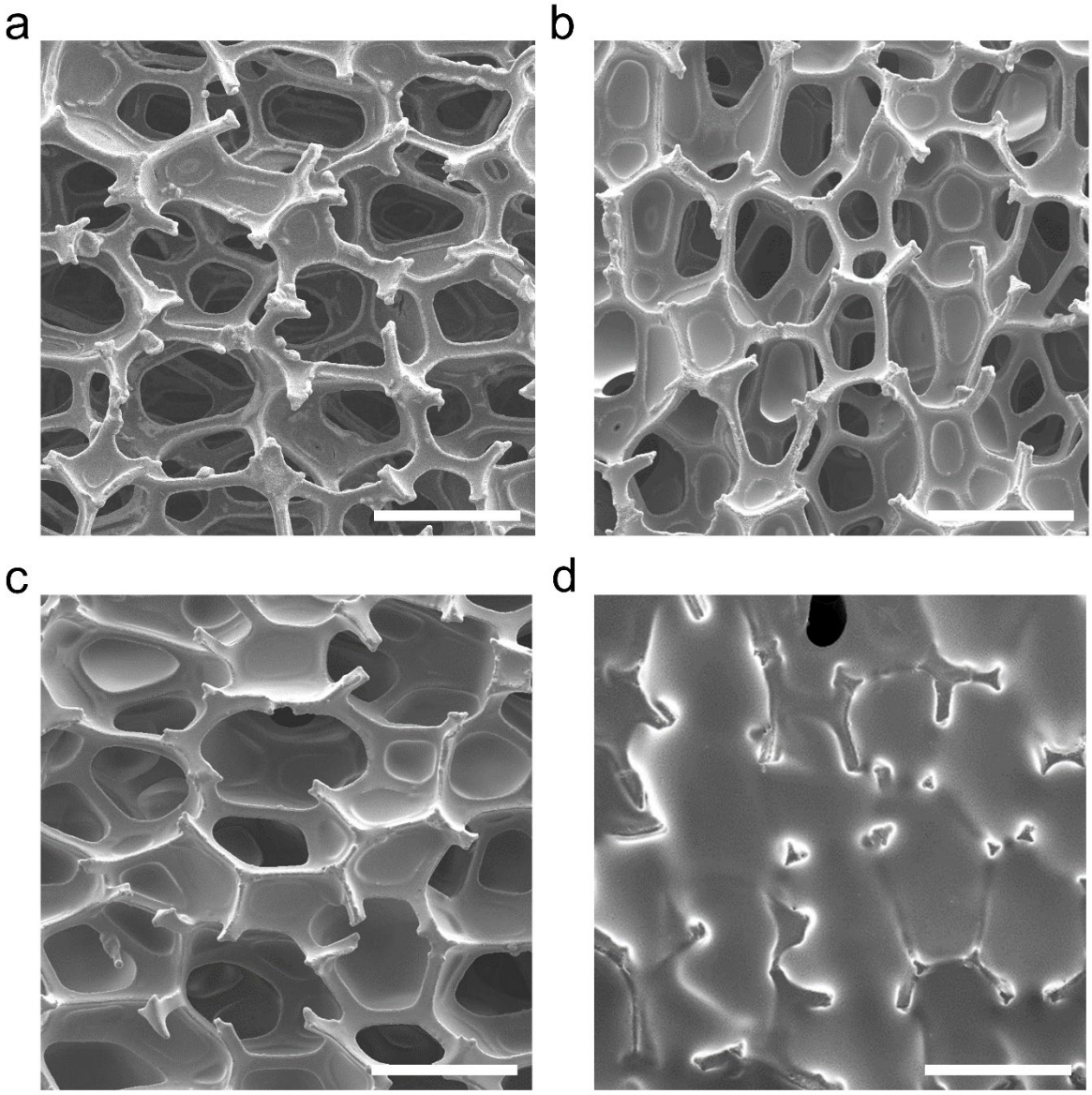

Figure S3 FE-SEM images of 3D Cu corresponding to different feeding amounts of PS-*b*-P2VP. The loaded PS-*b*-P2VP shown in (a), (b), (c), and (d) correspond to bf-mG-2, bf-mG-11, bf-mG-19, and bf-mG-32, respectively, after conversion to m-G. (all scale bars : 500 μm)

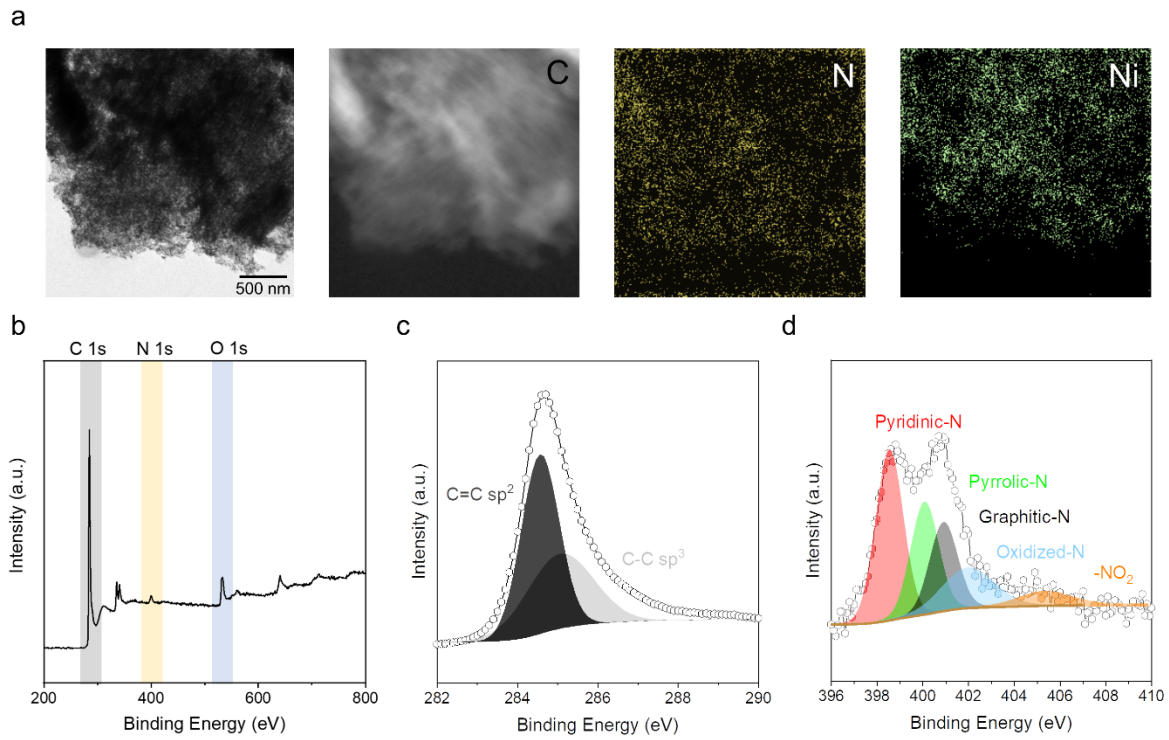

Figure S4 (a) TEM image and EELS mapping of m-G. The EELS mapping indicates that the elements C, N, and Ni elements are uniformly distributed within m-G, where the nitrogen originates from the pyridinic group of P2VP. (b) XPS survey spectrum. Enlarged (c) C 1s and (d) N 1s spectra. Meanwhile, the enlarged C 1s and N 1s spectra in Figure S4b shows that the bf-mG is primarily composed of sp^2 carbon, along with doped nitrogen atoms.

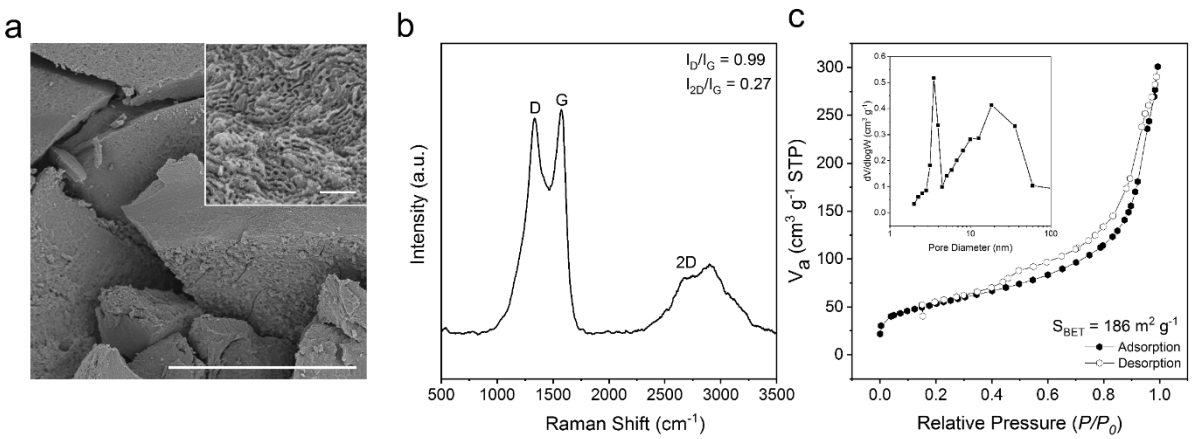

Figure S5 Characterization of m-G powder. (a) FE-SEM image of m-G powder (scale bar : 50 μm, and inset : 300 nm), (b) Raman spectrum, and (c) Nitrogen adsorption-desorption isotherm curve (inset: pore size distribution). The morphology and degree of graphitization are similar to those in m-G@3D Cu.

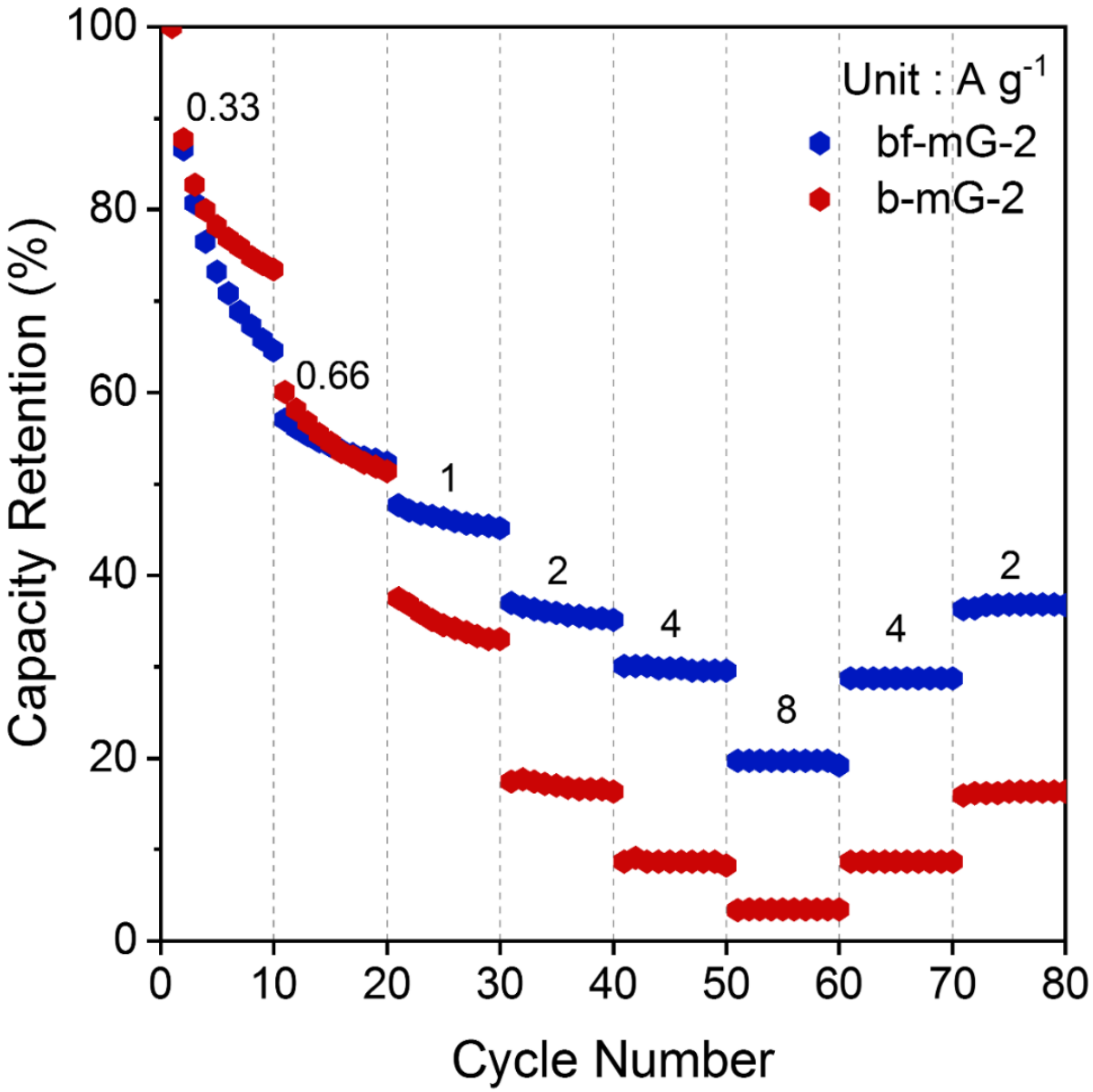

Figure S6 Capacity retention of bf-mG-2 and b-mG-2. During solid electrolyte interphase (SEI) formation in early cycles, the capacity retention of both bf-mG and b-mG decrease rapidly and stabilize afterwards. Capacity retention of bf-mG-2 is higher than b-mG-2.

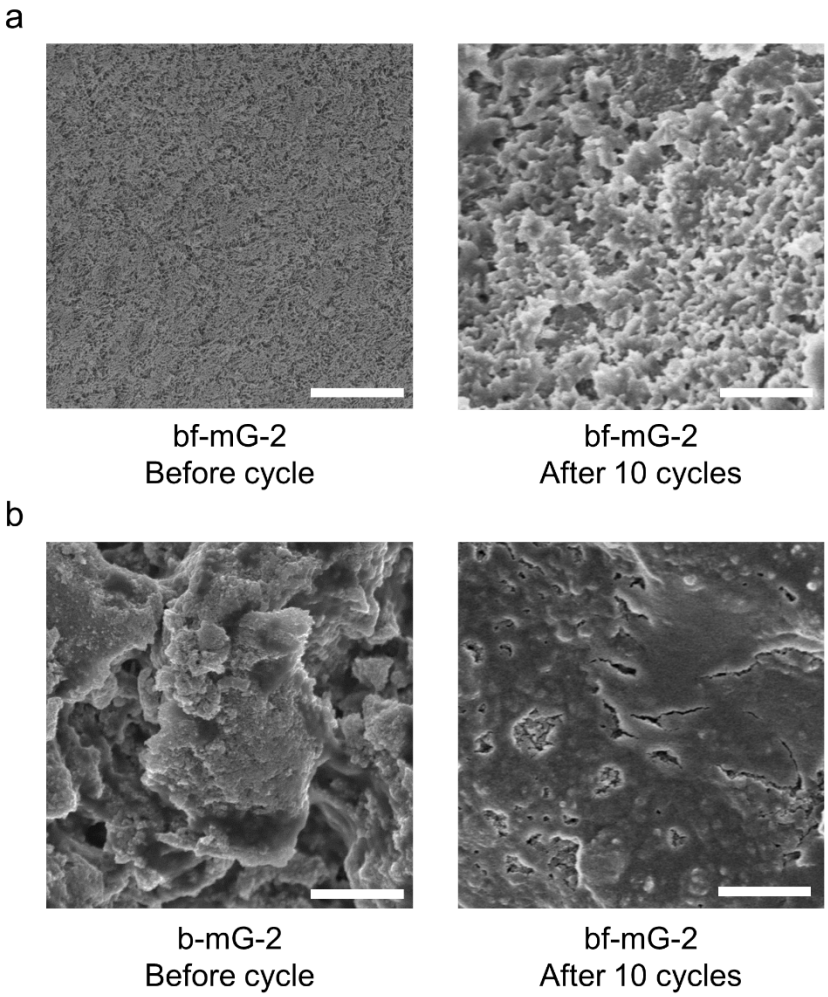

Figure S7 FE-SEM images of bf-mG-2 and b-mG-2: (a) bf-mG-2 before cycling and after 10 cycles at a current density of 0.33 A g^{-1}. (b) b-mG-2 before cycling and after 10 cycles at a current density of 0.33 A g^{-1} (Scale bar = 2 μm).

bf-mG-2 formed a porous SEI structure due to uneven SEI formation (Figure S7a). In contrast, for b-mG-2, a uniform and dense SEI was formed after 10 cycles due to the presence of a binder (Figure S7b). The dense SEI might hinder Li-ion transport to the m-G, whereas the porous SEI structure facilitates Li-ion transport to the m-G.

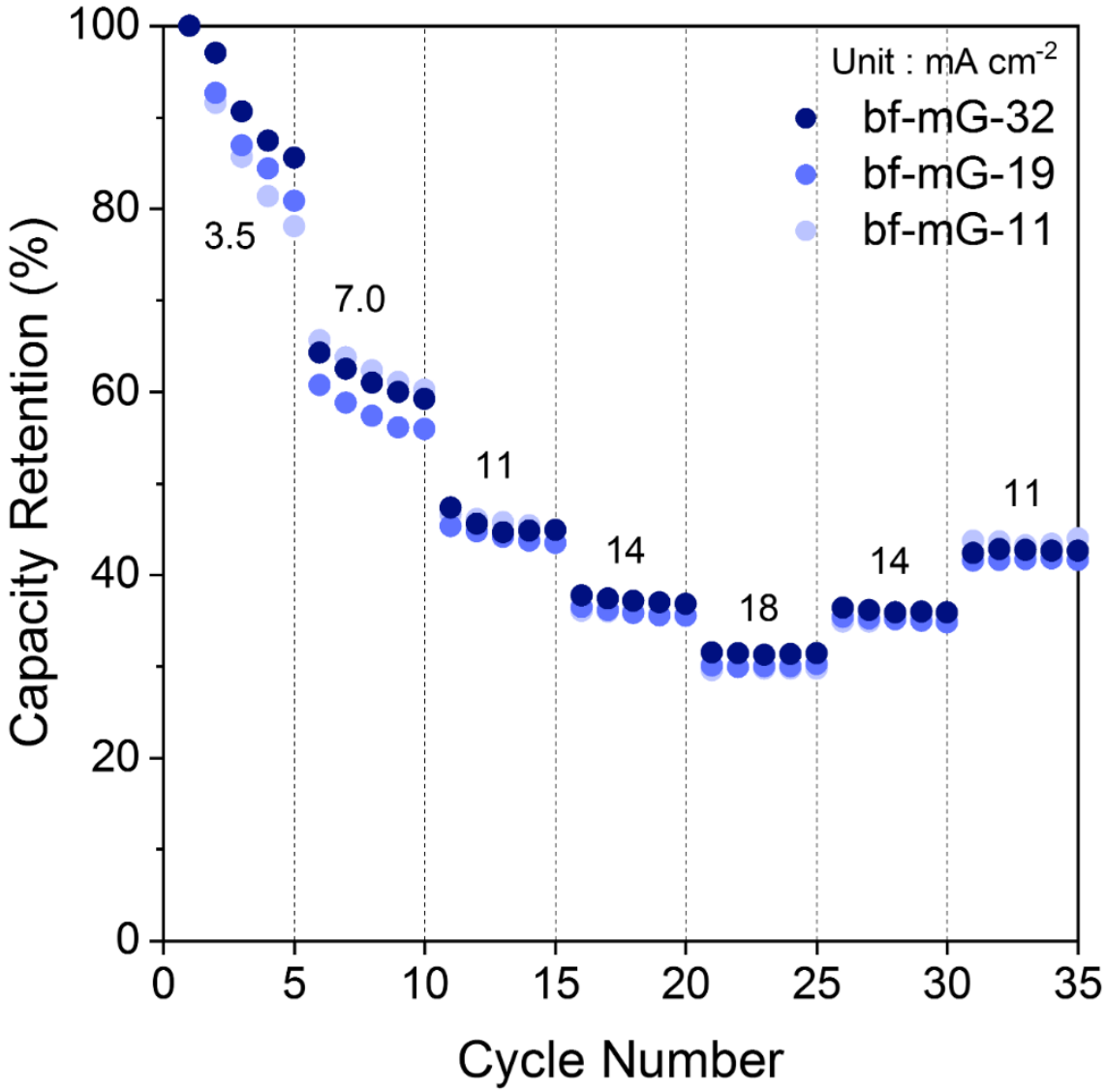

Figure S8 Capacity retention comparison of bf-mG with three different areal mass loading of m-G (11 mg cm^{-2}, 19 mg cm^{-2}, and 32 mg cm^{-2}). Capacity retention is similar regardless of the areal current density and areal mass loading.

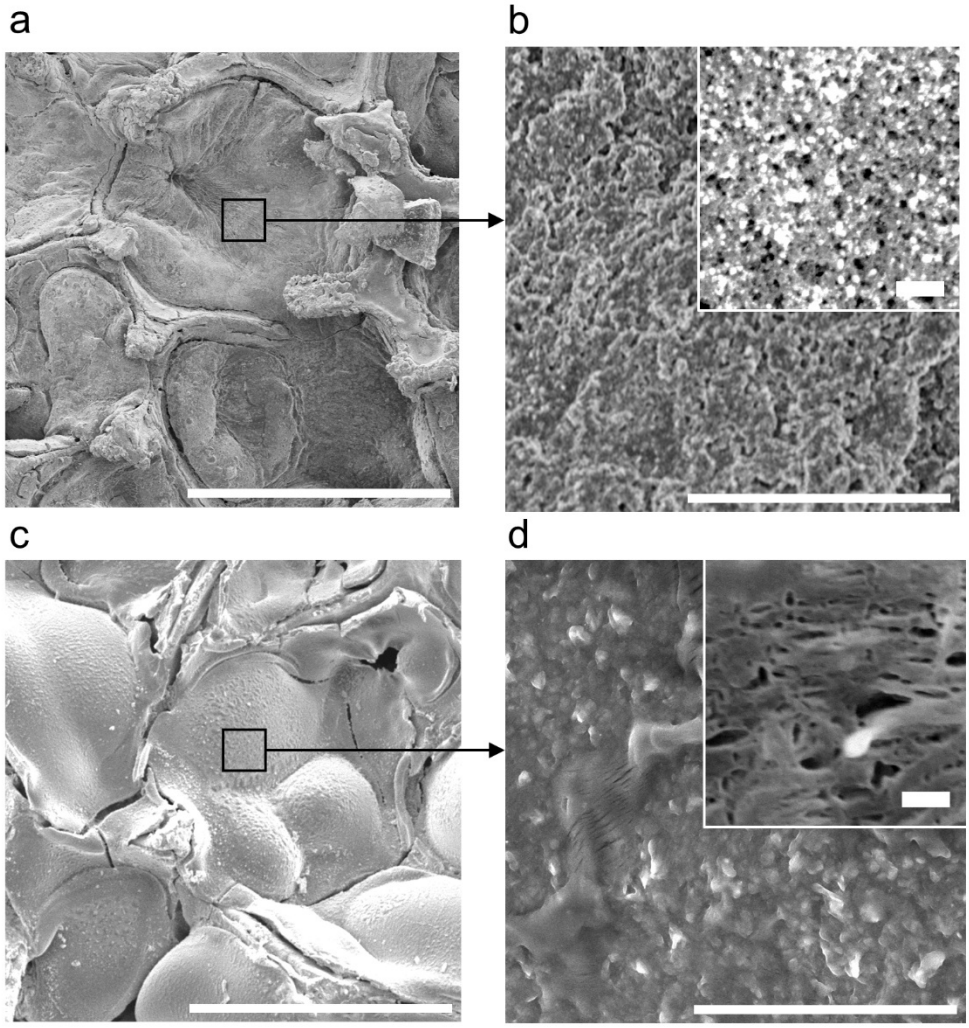

Figure S9 FE-SEM images of the bf-mG-32 after two different charge/discharge cylclings at a current density of 11 mA cm^{-2}: (a) after 10 cycles (scale bar = 500 μm), and (b) the magnified view (scale bar = 10 μm), along with a high-resolution inset (scale bar = 100 nm). (c) after 100 cycles (scale bar = 500 μm), and (b) the magnified image (scale bar = 10 um), along with a high-resolution inset (scale bar = 100 nm).

Figure S9(a-b) presents FE-SEM images of bf-mG-32 after 10 cycles. After 10 cycles, the loaded m-G retained its mesoporous structure due to the formation of substantial SEI layers. The formation of SEI in a wide area, facilitated by the large surface area of m-G, preserves its porous structure and thus enables efficient Li-ion transport. Even after 100 cycles, although the m-G displayed a slightly swollen morphology, it is stably attached to the 3D Cu framework without detachment (Figure S9c), ensuring effective electron transport to the loaded m-G. Additionally, while the mesopores on the m-G surface were more blocked compared to those obtained after 10 cycles (Figure S9d), the mesoporous structure retained, indicating that effective Li-ion transport can be maintained even after prolonged cycling.

References

1. J. Sacristan, H. Reinecke, C. Mijangos, S. Spells and J. Yarwood, *Macromol. Chem. Phys.* 2002, **203**, 678-685.